Chinese Journal of Structural Chemistry 43 (2024) 100247

Contents lists available at ScienceDirect

Chinese Journal of Structural Chemistry

journal homepage: www.journals.elsevier.com/chinese-journal-of-structural-chemistry

Article

Solid-state NMR study of the stability of MOR framework aluminum

Xinzhi Ding [a,c], Chong Liu [a], Jing Niu [a], Nan Chen [a,d], Shutao Xu [a,*], Yingxu Wei [a], Zhongmin Liu [a,b]

[a] National Engineering Research Center of Lower-Carbon Catalysis Technology, Dalian Institute of Chemical Physics, Chinese Academy of Sciences, Dalian, 116023, China
[b] State Key Laboratory of Catalysis, Dalian Institute of Chemical Physics, Chinese Academy of Sciences, Dalian, 116023, China
[c] University of Chinese Academy of Sciences, Beijing, 100049, China
[d] School of Chemistry, Dalian University of Technology, Dalian, 116024, China

ARTICLE INFO

Keywords:
H-MOR
Solid-state NMR
H_2O
Framework aluminum stability
Dealumination

ABSTRACT

MOR zeolite has been effectively utilized for dimethyl ether (DME) carbonylation reaction due to its unique pore structure and acidity. During industrial production, the transformation of ammonium type MOR zeolite (NH_4-MOR) into proton type MOR zeolite (H-MOR) causes inevitable dealumination. Therefore, understanding the influencing factors and dynamic evolution mechanism of zeolite dealumination is crucial. In this work, the stability of framework aluminum was studied by X-ray diffraction (XRD), Fourier transform infrared (FT-IR) spectroscopy, ^{29}Si, ^{27}Al, ^{1}H magic angle spinning nuclear magnetic resonance (MAS NMR), and DME carbonylation performance evaluation. These results indicate that extra-framework cation Na^+ and NH_4^+ could better preserve the aluminum structure of the MOR zeolite framework compared to H^+, primarily due to the different 'attraction' of the framework to water. Furthermore, the impact of water on the zeolite framework aluminum at high temperature was studied by manipulating the humidity of the calcination atmosphere, revealing the formation of extra-framework six-coordinated aluminum (Al(VI)-EF) and the mechanism of water influence on the zeolite framework aluminum.

1. Introduction

Zeolite, a microporous crystal material formed by the combination of TO_4 tetrahedra (T atoms usually refer to tetrahedrally coordinated Si, Al, or P) as the basic structural unit in strict accordance with the rules of crystallographic symmetry, plays a very important role in the field of catalysis [1–8]. Using coal-based syngas as a raw material, the process route for ethanol production through DME carbonylation and hydrogenation is a unique environmentally friendly new technology pathway. Due to the unique pore structure and acidity, MOR zeolites have been the most active and selective catalysts in DME carbonylation [9–14]. They have four crystallography unequal T sites (T1, T2, T3, T4) and ten O sites, and there are oval 12-membered ring straight channels (12-MR, 0.67 nm × 0.70 nm) and 8-membered ring narrow channels (8-MR, 0.28 nm × 0.57 nm) in the [001] direction, connected by 8-membered ring channels (8-MR, 0.34 nm × 0.48 nm) in the [010] direction, which are called side pockets [15,16]. The Brønsted acid sites in 8- and 12-MR exhibit different confined catalytic effects on the DME reactant. Theoretical calculations proved that the T3 site of 8-MR of MOR zeolites is the active site of DME carbonylation, and its confined environment is conducive to the formation of acetyl groups on the surface of CO insertion. The acid position in 12-MR is the reaction center of MTO (methanol-to-olefin) and other side reactions, and its confined environment is conducive to the formation of inactivation intermediates [13,17]. In DME carbonylation reaction, DME firstly interacts with bridge hydroxyl Si(OH)Al to form the surface methoxy group and methanol, then CO is inserted into the methoxy group in 8-MR to generate acetyl group which reacts with another DME molecule to form methyl acetate [18–22]. Acetyl active species have been spectrally confirmed by solid-state NMR technology, providing sufficient evidence for the above mechanism [23,24].

The widespread application of zeolites in industrial catalysis is mainly due to their strong acidity. When H^+ balances the framework negative charge brought by the AlO_4^- tetrahedron, zeolites generate a bridge hydroxyl group and thereby form a Brønsted acid center [25]. The location of the framework aluminum atom in zeolites determines the position of the catalytic acidic site, which influences the catalytic performance of the zeolites. Furthermore, some specific extra-framework aluminum species usually act as Lewis acid centers which also play an important role in

* Corresponding author.
E-mail address: xushutao@dicp.ac.cn (S. Xu).

https://doi.org/10.1016/j.cjsc.2024.100247
Received 1 January 2024; Received in revised form 6 February 2024; Accepted 6 February 2024
Available online 19 February 2024

cracking reactions and biomass conversion reactions [26–28]. Under certain conditions, these two acid centers can convert into each other. However, the structural versatility of aluminum results in many aluminum species [29–31], thus leading to a plurality of potential Lewis acid sites. At present, a variety of methods have been developed to improve the carbonylation reaction performance, such as changing the particle size of MOR zeolites [32], ion exchange [33,34], pyridine modification in zeolite channels [35,36], water vapor, and acid or alkali treatment [37,38], to increase the distribution of Brønsted acid in 8-MR. In practical industrial applications, the dealumination phenomenon often inevitably occurs in the process of NH_4-MOR calcining to H-MOR zeolites, resulting in the density decrease of zeolites Brønsted acid, and thus lowering the catalytic activities for DME carbonylation reaction. In 1991, researchers investigated different dealumination methods on various zeolites, including thermal treatment, complexation by oxalic acid and direct replacement of aluminum with gaseous silicon tetrachloride [39]. In conclusion, the identification of aluminum species in post-treatment and calcining process of zeolites, the stability of zeolite framework aluminum, and the microstructure evolution mechanism from framework aluminum to extra-framework aluminum in the process of dealumination are worthy of in-depth study.

In this study, MOR zeolite catalysts were investigated through sodium ion exchange and calcination under different humidity atmospheres. The effects of different extra-framework cations such as Na^+, NH_4^+ and H^+ on the stability of framework aluminum were carefully investigated by a combination of XRD, FT-IR, ^{29}Si, ^{27}Al, ^1H MAS NMR, and the evaluation of carbonylation of DME. Then the effect of water on the framework aluminum of zeolite was investigated at high temperature by manipulating the humidity in the calcination atmosphere. Based on these results, we elucidated the reason for the formation of Al(VI)-EF and proposed the mechanism to explain the effect of water on the framework aluminum of zeolites.

2. Results

2.1. Impact of cation types: the origin of four-coordinated framework Al(IV)-2 and six-coordinated framework Al(VI)

The corresponding topological structure of MOR zeolite was obtained (Figs. S1 and 2). After sodium ion exchange, the sample maintained good crystallinity and exhibited a slight increase in crystallinity (Table 1), indicating that sodium ion has a certain protective effect on the framework of MOR zeolites. Scanning electron microscope (SEM) results (Fig. S3) demonstrated that the morphology and size of the three samples remained almost unchanged, with all samples composed of plate crystal clusters with a size ranging from 200 to 300 nm. This shows that ion exchange has minimal effect on the morphology of MOR zeolites.

Solid-state NMR technology has been widely used in structural characterization, acidity characterization, and reaction mechanism of zeolites [40–43]. ^{27}Al MAS NMR spectroscopy was employed to investigate the samples with various degrees of sodium ion exchange (denoted as xNa/(100 − x)NH_4-MOR and xNa/(100 − x)H-MOR) after calcination. Fig. 1(a) shows the ^{27}Al MAS NMR spectra of sodium-ammonium mixed type MOR zeolites with different sodium ion exchange degrees, denoted as xNa/(100 − x)NH_4-MOR (x = 5, 9, 15 and 22). In all cases, only a symmetrical peak at 56 ppm corresponding to a four-coordinated framework aluminum (Al(IV)-1) was observed. Fig. 1(b) shows the ^{27}Al MAS NMR spectra of sodium-proton mixed type MOR zeolites formed from calcined sodium-ammonium mixed type samples with varying degrees of sodium ion exchange, denotes as xNa/(100 − x)H-MOR (x = 5, 9, 15, and 22). As the concentration of Na^+ decreases, the intensity of Al(IV)-1 signal decreases accompanied by a certain degree of broadening and the symmetry drops. Furthermore, the signals of Al(IV)-1 (55 ppm), Al(IV)-2 (40–50 ppm) and Al(VI) (near 0 ppm) were identified by ^{27}Al multiple quantum (MQ) MAS NMR experiment (Fig. 1(c)). No signal for pentahedral aluminum Al(V) is detected. Distorted tetrahedral and pentahedral aluminum can be clearly distinguished in terms of their chemical shifts [44]. Furthermore, according to previous reports [45], signals for Al(V) can only be detected in MOR zeolite at calcination temperatures above 650 °C, while our calcination temperature is 550 °C. The Al(IV)-2 signal, previously referred to as 'DTetrAl' [46] and classified in the literature as a distorted four-coordinated aluminum species containing one or more Al–OH bonded to the framework part [29,30,47], showed a gradual decrease in signal intensity when increasing the Na^+ concentration. These results indicate that the framework structure of zeolite changes to a certain extent during calcination from NH_4^+- to H^+-type zeolites, but the presence of Na^+ can protect the structure in different degrees. This occurrence has been documented in prior research, noting that the presence of ions such as Na^+ or Cu^{2+} can lead to a reduction of dealumination to some extent or even complete inhibition of the process [48]. Notably, the protective effect increases with higher Na^+ concentration, suggesting that the existence of Na^+ enhances the aluminum stability of MOR zeolite framework. The samples with different Na^+ exchange degrees (xNa/(100 − x)H-MOR) were characterized by ^{29}Si MAS NMR. In Fig. 1(d), the signals at −99, −102 and −106 ppm correspond to the framework Si(2Al), Si–OH and Si(1Al) species, respectively. And the signals at −112 and −114.5 ppm are attributed to Si(0Al) species, which are not equivalent in crystallography [49–51]. By fitting the spectra with Gauss-Lorentz peak separation, the framework Si/Al ratios of 5Na/95H-MOR, 9Na/91H-MOR, 15Na/85H-MOR and 22Na/78H-MOR samples were determined with the values of 8.9, 8.9, 8.4, and 8.0, respectively (Table 1), which also shows that Na^+ can protect the framework aluminum atom of MOR zeolite with almost no dealumination.

Further studies have been carried out on the formation of twisted Al(IV)-2 and Al(VI) species [52]. This was achieved by NH_4^+ re-exchange experiment on samples xNa/(100 − x)H-MOR, producing xNa/(100 − x)H-MOR-NH_4^+ (x = 5, 9, 15, 22) samples (after re-exchange, they become the proton type MOR zeolite). Subsequently, the ^{27}Al MAS NMR spectra of xNa/(100 − x)NH_4-MOR, xNa/(100 − x)H-MOR and xNa/(100 − x)H-MOR-NH_4^+ samples were compared, as shown in Fig. 2(a). In the case of samples with different Na^+ contents after NH_4^+ re-exchange (5Na/95H-MOR-NH_4^+, 9Na/91H-MOR-NH_4^+, 15Na/85H-MOR-NH_4^+ and 22Na/78H-MOR-NH_4^+, Figs. S4–6), the signals of Al(IV)-2 and Al(VI) disappeared, and the intensity of Al(IV)-1 signal peak increased, indicating the transformation of Al(VI) and Al(IV)-2 into Al(IV)-1 species after ammonium ion (NH_4^+) re-exchange, which also implies that the Al(VI) produced after calcination belongs to the octahedral framework aluminum Al(VI)-F. Because the sample was exposed to air before ^{27}Al MAS NMR experiments, the signal of the six-coordinated framework aluminum (Al(VI)-F) detected on the ^{27}Al MAS NMR spectra of the sample calcined in the tube furnace may be caused by the interaction of a portion of the water in air with the zeolite framework. In order to validate this hypothesis, deamination and dehydration treatments of xNa/(100 − x)NH_4-MOR (x = 5, 9, 15, 22) samples were performed on the vacuum line at 823 K to eliminate the influence of water. Subsequently, the ^{27}Al MAS NMR experiment was conducted, with the results shown in Fig. 2(b). Obviously, only Al(IV)-1 signals and a few Al(IV)-2 signal peaks were observed in four samples, while the Al(VI) signal disappeared. This observation indicates that the formation of 0 ppm signal of Al(VI)-F results from the interaction between water and

Table 1
The physicochemical properties of xNa/(100 − x)H-MOR (x = 5, 9, 15, 22).

Sample	CXRD (%)	Si/Al ratio[a]	^1H MAS NMR (mmol/g)		
			BAS	Al–OH	Si–OH
5Na/95H-MOR	91.8	8.9	1.18	0.07	0.02
9Na/91H-MOR	94.3	8.7	1.12	0.08	0.02
15Na/85H-MOR	94.6	8.4	1.06	0.06	0.02
22Na/78H-MOR	94.4	8.0	1.02	0.07	0.02

[a] Framework Si/Al ratios obtained by ^{29}Si MAS NMR experiments.

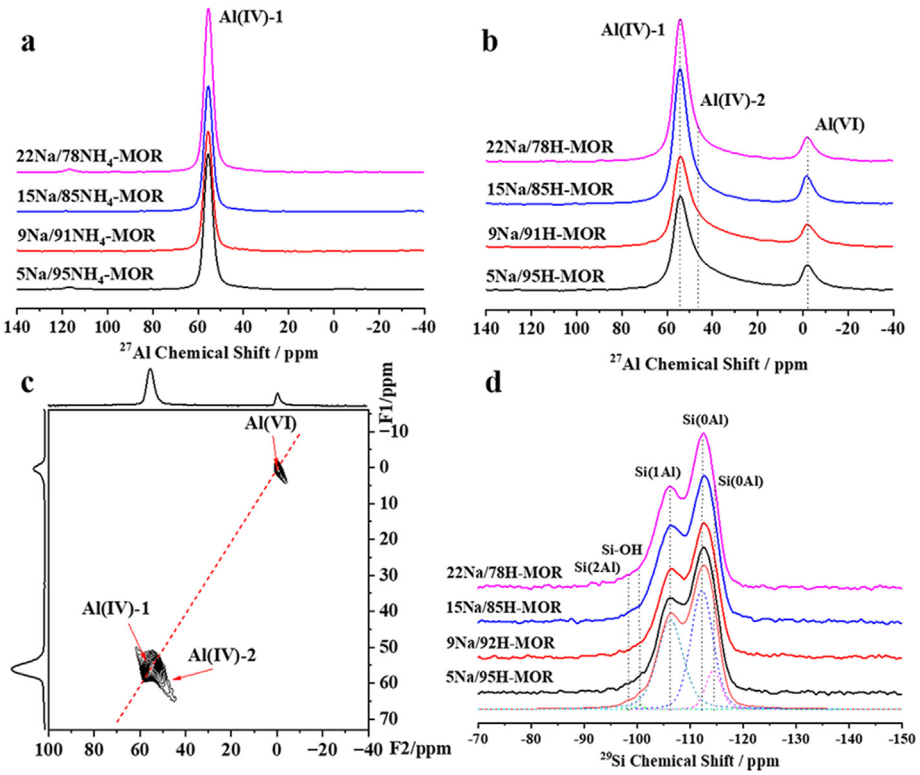

Fig. 1. (a, b) ^{27}Al MAS NMR spectra for (a) xNa/(100 − x)NH_4-MOR (x = 5, 9, 15, 22) and (b) xNa/(100 − x)H-MOR (x = 5, 9, 15, 22), (c) ^{27}Al MQ MAS NMR spectra of 5Na/95H-MOR, (d) ^{29}Si MAS NMR spectra of xNa/(100 − x)H-MOR (x = 5, 9, 15, 22).

framework aluminum, and this effect is reversible because the AlO_4^- tetrahedron in MOR zeolite has one unit of negative charge and consequently, cations are needed to balance the charge before ^{27}Al MAS NMR experiments. Compared with H^+, Na^+ and NH_4^+ exhibit lower polarity and weaker affinity to water, explaining why Na^+ and NH_4^+ typed samples have no Al(VI)-F signal while it appears in the H^+ typed one.

The acidity of four samples with different sodium ion exchange degree (xNa/(100 − x)H-MOR) was studied by ^{1}H MAS NMR experiment, as shown in Fig. 3. Signals at 3.9, 2.6 and 1.8 ppm were assigned to bridging hydroxyl group (Brønsted acid site), Al–OH species and non-acidic Si–OH species, respectively [34,52]. By fitting the ^{1}H MAS NMR spectra, the total amount of Brønsted acid of the four samples was determined. As shown in Table 1, the Brønsted acid densities of 5Na/95H-MOR, 9Na/91H-MOR, 15Na/85H-MOR and 22Na/78H-MOR samples are 1.18, 1.12, 1.06 and 1.02 mmol/g, respectively. With the increase of sodium ion exchange degree, the Brønsted acid density of zeolites decreases due to the fact that Na^+ replaces part of NH_4^+ during ion exchange and thus leads to a reduction of the Brønsted acid density of the zeolite sample after calcination. Additionally, the intensity of Al–OH and Si–OH peaks almost remained nearly unchanged, indicating no significant dealumination during the calcination process, consistent with the ^{29}Si MAS NMR results.

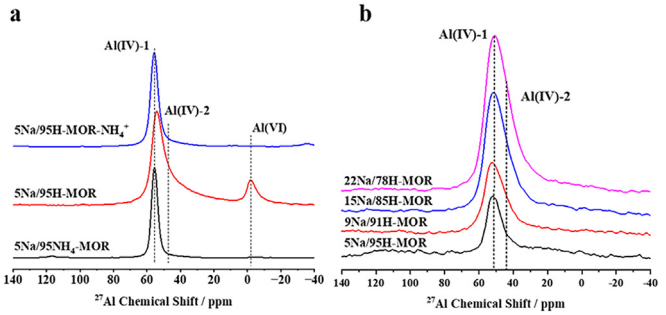

Fig. 2. (a, b) ^{27}Al MAS NMR spectra of (a) MOR samples with different treatment conditions and (b) xNa/(100 − x)H-MOR (x = 5, 9, 15, 22) after dehydration.

2.2. *Impact of calcination conditions: the origin of six-coordinated extra-framework aluminum Al(VI)-EF*

As mentioned earlier, the origin of Al(VI)-F (0 ppm) arises from the interaction between water and framework aluminum, and this effect is reversible. Under the previous experimental conditions, this conclusion is limited by the interaction of water with the zeolite framework aluminum

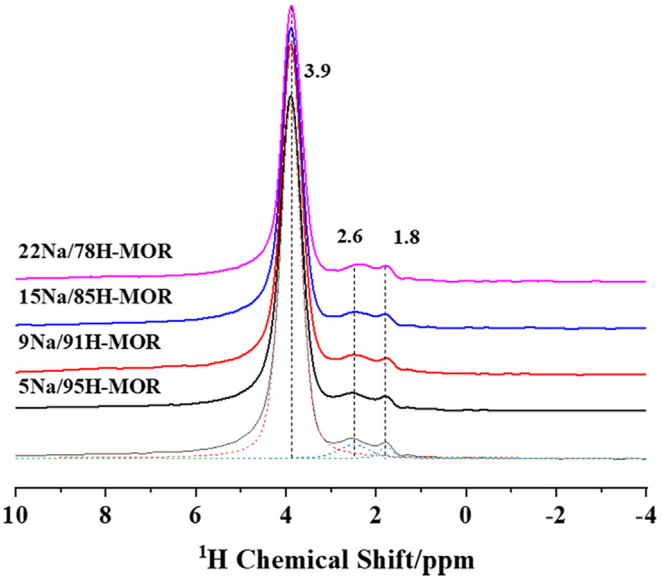

Fig. 3. ^{1}H MAS NMR spectra of xNa/(100 − x)H-MOR (x = 5, 9, 15, 22).

at room temperature. In order to investigate the effect of water at higher temperature on the macroscopic and microscopic crystal structure of MOR zeolite, NH_4-MOR, HMOR-1, HMOR-2 and HMOR-3, it's essential to note the distinct calcination conditions for these samples. HMOR-1 was calcined in a vacuum environment, HMOR-2 in a tube furnace filled with dry air dehydrated by silicone gel, and HMOR-3 in a muffle furnace environment with ambient air in the laboratory, with their difference to be the humidity of calcining atmosphere. XRD results show that the characteristic MOR zeolite topology persisted in all samples, indicating that the framework structures of the zeolites remain unchanged after calcination under three environments. Particularly noteworthy is the slight increase in relative crystallinity of the samples after calcining under vacuum conditions (Fig. S7). The SEM results show that the morphology and size of the samples before and after calcining exhibited minimal alterations, which are all clustered by plate-like crystals with a size of 200~300 nm (Fig. S8). These observations indicate that the diversity of calcining conditions, including vacuum, tube furnace and muffle furnace environments, has negligible effects on the macroscopic morphology of the MOR zeolite.

In order to further investigate the effect of water at high temperature on the zeolite framework aluminum, the above three samples were characterized by ^{27}Al MAS NMR. Fig. 4(a) shows the ^{27}Al MAS NMR spectra of them after water absorption. Signals at 55, 40–50 and 0 ppm were attributed to the Al(IV)-1, twisted Al(IV)-2 and Al(VI) signal, respectively. Fig. 4(a) illustrates a discernible trend in the peak intensity of Al(IV)-1 in the three samples. Evidently, the peak intensity of Al(IV)-1 gradually decreases, while a concomitant increase is observed in that corresponding to the twisted Al(IV)-2 signal. Fig. 4(b) shows the ^{27}Al MAS NMR spectra of NH_4^+ re-exchange HMOR samples, named HMOR-*x*-NH_4^+ ($x = 1$, 2 and 3). For HMOR-1-NH_4^+ and HMOR-2-NH_4^+ samples, the disappearance of Al(VI) signal indicates that majority of the generated Al(VI) signals after calcining are Al(VI)-F, with only a trace of Al(VI)-EF. On the contrary, for HMOR-3-NH_4^+ samples, the clear presence of Al(VI) signal suggests a more substantial production of Al(VI)-EF after muffle furnace calcining, which proves that part of the framework of the sample calcined in the muffle furnace environment is damaged, and the extent of damage increases in the presence of higher moisture content in air. In addition, in previous work [44,52,53], counter ion exchange experiments were carried out on NH_4NO_3 for H-MOR obtained at different calcining temperatures in tube furnaces, demonstrating a decrease in the signal intensity of Al(VI) in H-MOR zeolite. However, the signal does not entirely disappear after NH_4^+ re-exchange, proving evidence for the existence of Al(VI)-EF. In order to further investigate the effect of water at high temperatures on the structure of zeolite framework, a ^{29}Si MAS NMR characterization was performed, with the results shown in Fig. 4(c) in which a gradual decease in the peak intensity of Si(1Al) signal from HMOR-1 to HMOR-3 indicates that the framework Si/Al ratios of these three samples are increasing sequentially. By fitting the Gauss-Lorentz peaks to the spectra, such ratios were derived and summarized in Table 2, 10.4, 11.2 and 12.6 for HMOR-1, HMOR-2 and HMOR-3, respectively. The results indicate that under calcination conditions of both tube and muffle furnaces, the presence of water has an impact leading to the partial destruction of zeolite framework structures and an increase in the Si/Al ratio of the framework. Although there is still a trace amount of water present in the air during calcination in the tube furnace, its influence is significantly less than that of the samples calcined in the air atmosphere of the muffle furnace. The occurrence of Al(VI)-EF indicates that water will cause irreversible transformation of framework aluminum at high temperature, different from the reversible change caused by water at room temperature.

The acidic properties of calcined samples under different air atmospheres were quantitatively studied by ^{1}H MAS NMR combined with FT-IR spectroscopy (Fig. S9). As shown in Fig. 4(d), the total amount of Brønsted acid for the three samples can be obtained by peak fitting of the

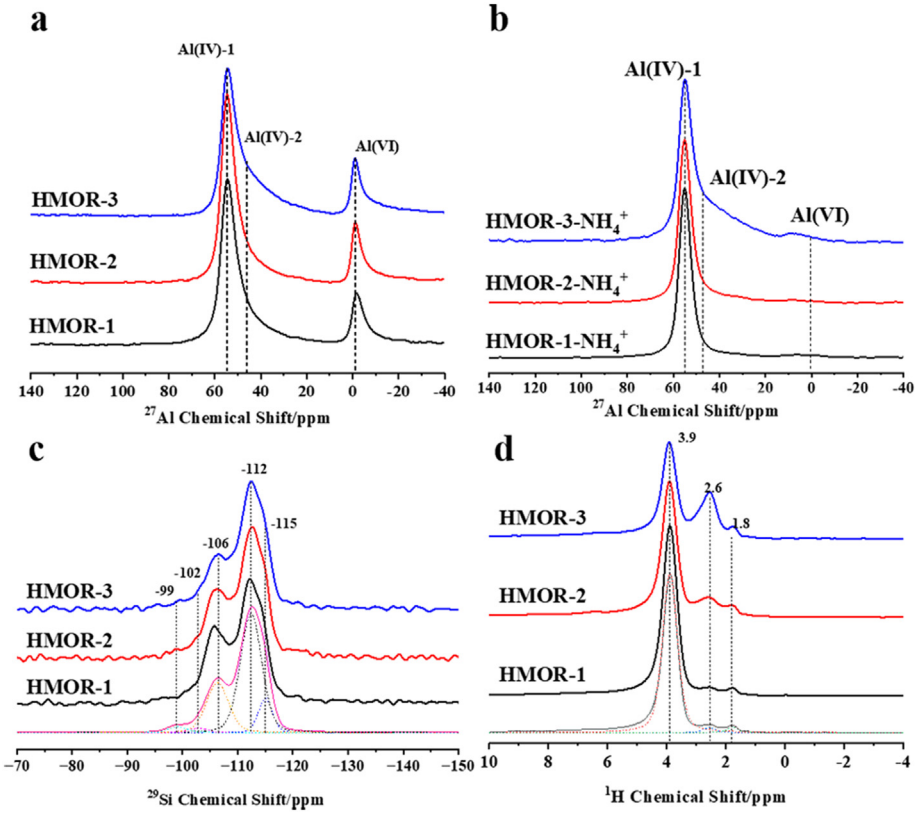

Fig. 4. (a) ^{27}Al MAS NMR spectra of HMOR-1, HMOR-2 and HMOR-3 after water absorption; (b) ^{27}Al MAS NMR spectra of HMOR-1, HMOR-2 and HMOR-3 samples with NH_4^+ re-exchange after water absorption; (c) ^{29}Si MAS NMR spectra of HMOR-1, HMOR-2 and HMOR-3; (d) ^{1}H MAS NMR spectra of HMOR-1, HMOR-2 and HMOR-3.

Table 2
Physicochemical properties of HMOR-1, HMOR-2 and HMOR-3.

Sample	CXRD (%)	Si/Al ratio[a]	^{1}H MAS NMR (mmol/g)			FT-IR[b]	
			BAS	Al–OH	Si–OH	8-MR	12-MR
HMOR-1	101.8	10.4	1.35	0.04	0.03	0.77	0.58
HMOR-2	93.0	11.5	1.35	0.20	0.04	0.62	0.46
HMOR-3	97.4	12.6	1.08	0.44	0.03	0.43	0.33

[a] Framework Si/Al ratio, obtained by ^{29}Si MAS NMR experiments.
[b] The Brønsted acid content of 8-MR and 12-MR was obtained by combining FT-IR spectroscopy and ^{1}H MAS NMR.

^{1}H MAS NMR spectrum. The Brønsted acid densities of HMOR-1, HMOR-2 and HMOR-3 samples are 1.35, 1.08 and 0.76 mmol/g, respectively (Table 2). Therefore, the Brønsted acid density of tubular and muffle furnace calcining environment is lower than that in vacuum, which once again proves that the joint influence of water and high temperature leads to the destruction of part of the framework structure of zeolite. In addition, the concentration of Al–OH species in the HMOR-1 sample was 0.04 mmol/g, indicating basically no dealumination phenomenon appears in the calcined zeolite under vacuum environment. The Brønsted acid distribution ratios of 12-MR and 8-MR in H-MOR zeolite were obtained by FT-IR spectroscopy. Combined with the total amount of Brønsted acid given by ^{1}H MAS NMR, the Brønsted acid contents of 12-MR and 8-MR can be further obtained, with the results listed in Table 2. It can be seen that the HMOR-1 sample has more Brønsted acid content in both total acid content and 8-MR than other samples, indicating it may have relatively high DME carbonylation activity. Further verification is required through experiments on the carbonylation of DME.

The time-dependent curves of DME conversion and methyl acetate selectivity of HMOR-1, HMOR-2 and HMOR-3 are shown in Fig. 5, which shows three obvious stages of induction period, high efficiency period and inactivation period in the carbonylation process of DME. The methyl acetate formation rate of H-MOR increased rapidly after a short induction period and decreased rapidly after the highest point, indicating that the zeolite began to deactivate. In the initial stage of the reaction (1 h), the conversion rates of DME of HMOR-1, HMOR-2 and HMOR-3 were respectively 27.2%, 27.6% and 22.4%, all higher than 20%. After reacting for 2 h, the conversion of DME of HMOR-1 and HMOR-2 increased respectively to 38.7% and 36.8%, and that of HMOR-3 increased to 26.8%, which was the induction stage. Then the reaction experienced a relatively high efficiency conversion period of 2 h, and the catalyst began to deactivate. Among them, the highest conversion of DME

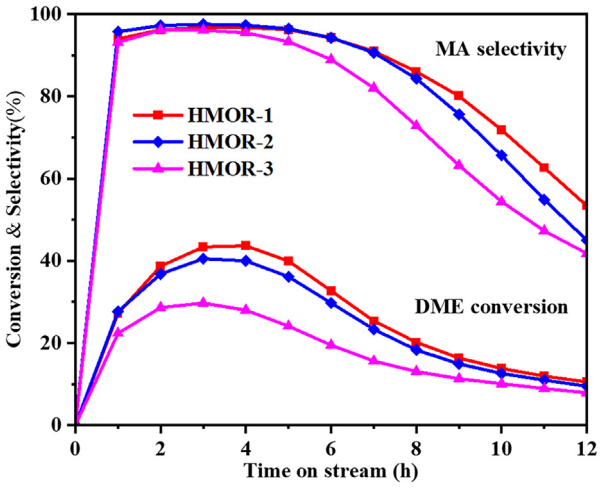

Fig. 5. DME conversion and MA (methyl acetate) selectivity as a function of time during DME carbonylation over HMOR-1, HMOR-2 and HMOR-3.

of HMOR-1 is 43.7%, followed by 40.5% for HMOR-2, which is close to that of HMOR-1, and then 29.7% for HMOR-3. Therefore, the activity order of carbonylation of DME is HMOR-1 > HMOR-2 > HMOR-3, consistent with the change of Brønsted acid concentration in the eight-membered ring. It shows that the co-existence of water and high temperature will cause irreversible damage to framework aluminum, which should be controlled to reduce the emergence of extra-framework aluminum. Therefore, calcining in vacuum and dry air (strict dehydration) can protect the framework aluminum to the greatest extent and improve the stability of the framework aluminum.

3. Conclusion

In this study, we investigate the stability of framework aluminum in MOR zeolite through various analytical techniques including XRD, FT-IR, ^{29}Si, ^{27}Al, ^{1}H MAS NMR, and DME carbonylation performance assessment. The summary of the work is presented in Fig. 6, and the structural representations of aluminum species mentioned in the figure are based on previous studies [31]. Various possibilities for Al(IV)-2 and Al(VI)-F arise from the fact that there could be multiple scenarios for the cleavage of Al–O–Si bonds, resulting in a diverse distribution of Al–OH groups after cleavage. As shown in Fig. 6, compared to H^+, the Na^+ and NH_4^+ ions better protect the aluminum structure within the MOR zeolite framework primarily attributed to variations in the framework's affinity for water. Furthermore, we explore the influence of water on zeolite framework aluminum at a calcination temperature of 550 °C, observing the formation of Al(VI)-EF by manipulating the humidity of the calcination atmosphere. Our investigation also sheds light on the mechanism by which water affects extra-framework aluminum. The interaction between water and framework aluminum results in the transformation of framework Al(IV)-1 into twisted Al(IV)-2, ultimately leading to the emergence of Al(VI)-F. Importantly, this transformation process is reversible. Under elevated temperatures, water induces irreversible deterioration in the framework aluminum structure, resulting in the creation of Al(VI)-EF. It's worth highlighting that, under Na^+ protection, the transformation of Al(IV) is limited to Al(VI)-F. These discoveries provide more reliable evidence for the characterization of aluminum species in the dealumination process, illuminating the complex mechanism governing the impact of water on the framework structure during the dealumination of MOR zeolite.

4. Experimental

4.1. Preparation of the catalysts

The zeolite material used in the experiment was pure Na-MOR (Si/Al = 8, containing a template) purchased from the Nankai Zeolite Catalyst Factory. Initially, the zeolite was calcined at 550 °C for 6 h in a muffle furnace to remove the template. Next, a solution of NH_4NO_3 with a concentration of 1 mol/L was prepared for ion exchange with Na-MOR zeolite. The ion exchange conditions of this stage were as follows: a water bath temperature of 80 °C, a total of 3 exchanges, each lasting for 2 h. After centrifugal washing, the samples were dried in an oven for 12 h to obtain NH_4-MOR samples. Different concentration gradients of $NaNO_3$ solutions were prepared for ion exchange with NH_4-MOR samples. Ion exchange conditions of this stage are a water bath temperature of 80 °C, single exchange and a duration of 2 h. After centrifugal washing, the samples were dried in an oven for 12 h to obtain sodium-ammonium mixed type MOR zeolite samples with varying sodium ion exchange degrees (xNa/(100 – x)NH_4-MOR). X-ray fluorescence (XRF) spectroscopy analysis revealed sodium ion exchange levels of 5%, 9%, 15% and 22% for the four samples named 5Na/95NH_4-MOR, 9Na/91NH_4-MOR, 15Na/85NH_4-MOR and 22Na/78NH_4-MOR, respectively. These samples were placed in a tube furnace and heated to 550 °C continuously for 4 h using a room temperature heating program in flowing dry air (100 mL/min), resulting in the formation of sodium-hydrogen mixed type MOR zeolite

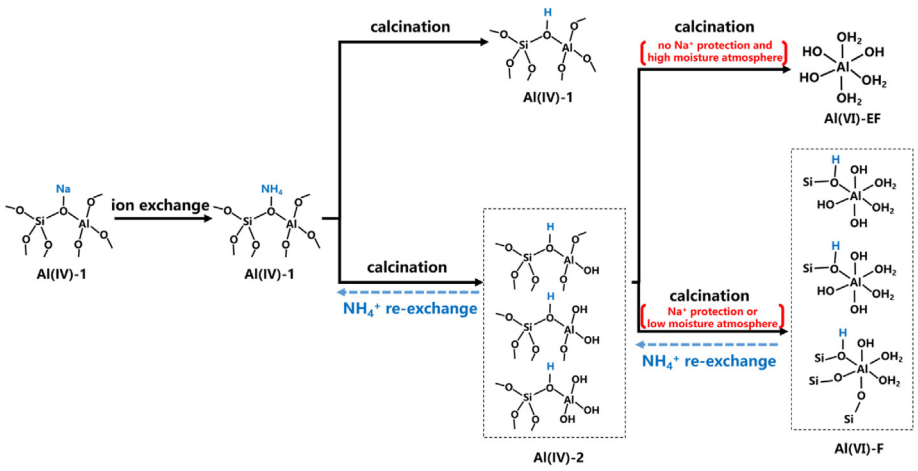

Fig. 6. Schematic representation of Al species structural evolution during ion exchange process and calcination in MOR zeolite. Some possible schematic structures of Al(IV)-1 and Al(VI)-F are shown in the dashed box.

samples: 5Na/95H-MOR, 9Na/91H-MOR, 15Na/85H-MOR and 22Na/78H-MOR. The steps for ammonium exchange experiment involve weighing 1 g of zeolite sample, adding it to an 80 mL solution of NH_4NO_3 with a concentration of 1 mol/L, and exchanging it at 80 °C for 5 h in a water bath. Subsequently, the samples were centrifuged and washed with deionized water at room temperature. The samples after NH_4^+ exchange were named 5Na/95H-MOR-NH_4^+, 9Na/91H-MOR-NH_4^+, 15Na/85H-MOR-NH_4^+ and 22Na/78H-MOR-NH_4^+. The previously obtained NH_4-MOR samples were subjected to calcining at 550 °C under different conditions, providing HMOR-1 in a vacuum environment, HMOR-2 in a tube furnace with dry air as the gas, and HMOR-3 in a muffle furnace environment with laboratory air as the gas.

4.2. Characterizations

All XRD experiments for the solid zeolite powder samples were conducted using the X'Pert PRO instrument from PANalytical in Netherlands under the following conditions: Cu target, Kα line radiation source with a wavelength of 1.5418 Å, operating voltage of 40 kV and current of 40 mA. The scanning range was from 5° to 60° at a scan rate of 5°/min.

Field emission SEM analysis was performed using the Hitachi SU8020 instrument at Hitachi Corporation in Japan to observe the size and morphology of the zeolite samples. Prior to testing, a small amount of the zeolite sample was dispersed onto a conductive adhesive and then transferred to the sample chamber, which was evacuated. The typical testing conditions were as follows: acceleration voltage of 2 kV, current of 10 mA, and working distance of 6 mm.

XRF was determined using the Magic-601 instrument from Philips in Netherlands to analyze the elemental composition of the zeolite samples. Prior to testing, the samples needed to undergo a pressing procedure to create pellets.

FT-IR experiments were conducted using the TENSOR 27 FT-IR spectrometer from Bruker in Germany. Initially, the powdered samples were pressed into self-supporting circular pellets with a diameter (φ) of 14 mm, placed in an *in-situ* infrared cell, and then pretreated in vacuum at 300 °C for 1 h to remove moisture from the samples. The temperature was then lowered to 50 °C for infrared spectrum scanning. The scanning range was from 4000 to 1000 cm^{-1} with 32 scans and a resolution of 4 cm^{-1}.

Solid-state NMR characterization experiments were conducted using the Bruker Advance NEO 500 (11.7 T) and Bruker Advance III 600 (14.1 T) spectrometers manufactured by Bruker in Switzerland. The ^1H MAS NMR spectra were acquired on the Bruker Advance NEO 500 (11.7 T) NMR spectrometer using a 3.2 mm H-X-Y triple-resonance probe, operating at a ^1H resonance frequency of 500.1 MHz. The experiment employed a one-pulse sequence with a spinning rate of 20 kHz, a power of 48 W, a π/2 pulse width of 3.8 μs, a pulse delay of 100 s and 8 scans. The chemical shifts were calibrated with adamantane as a reference, corrected to 1.74 ppm. Prior to testing, the samples were dehydrated under vacuum conditions ($< 10^{-3}$ Pa) and maintained at 420 °C for more than 12 h. After that, they were transferred into a glovebox for preparation. The quantification of the Brønsted acid density in the zeolite samples was performed using Gaussian-Lorentz line shape deconvolution fitting in DMFIT. Using adamantane as an external standard, the peak areas in the spectra were compared to normalize the sampling times and masses of the test samples. The hydrogen content in the zeolite samples was determined by comparing the peak areas through ^1H NMR. ^{29}Si MAS NMR experiments were conducted on the Bruker Advance NEO 500 (11.7 T) NMR spectrometer using a 4 mm H-X double-resonance probe with the ^{29}Si resonance frequency to be 99.4 MHz. A high-power proton decoupling sequence was employed with a spinning rate of 8 kHz, a power of 130 W, a sampling interval of 10 s, a π/4 pulse width of 2.2 μs and 512 scans. Chemical shifts were referenced to kaolin and calibrated to −91.5 ppm. ^{27}Al MAS NMR experiments were conducted on the Bruker Advance NEO 500 (11.7 T) NMR spectrometer using a 4 mm H-X double-resonance probe, and the ^{27}Al resonance frequency was 130.3 MHz. A one-pulse sequence was employed with a spinning rate of 12 kHz, a power of 88 W, a π/12 pulse width of 0.39 μs and a sampling interval of 1 s. Chemical shifts were referenced to a 1 mol/L $Al(NO_3)_3$ aqueous solution and calibrated to 0 ppm. The ^{27}Al MQ MAS NMR experiments were performed on the Bruker Advance III 600 MHz (14.1 T) NMR spectrometer using a 3.2 mm H-X probe. The experiments utilized the mp3qzqf sequence with a spinning rate of 20 kHz and a relaxation time of 0.5 s. The optimized pulse widths for the sequence were as below: the excitation pulse width (p1) was 4.5 μs, the conversion pulse width (p2) was 1.5 μs, and the selective pulse width (p3) was 17.5 μs.

4.3. Catalyst evaluation

The evaluation of DME carbonylation performance was conducted in a high-pressure fixed-bed reaction system. The catalyst loading was 0.2 g, with a particle size ranging from 40 to 60 mesh. The reaction conditions were as follows: under a nitrogen atmosphere (30 mL/min), the temperature was ramped up to 300 °C, and then held for 1 h for dehydration. Then the temperature was lowered to 200 °C, and the gas was switched to the reaction mixture (DME:CO:N_2 = 5:35:60). The reaction pressure was raised to 2.0 MPa, and the gas flow rate was set at 1800 mL/gcat./h. The gases produced in the reaction were separated using an Agilent 7890A gas chromatograph, and various compounds were detected using flame

ionization detector (FID) and thermal conductivity detector (TCD) detectors. The conversion of the reactant DME and the selectivity of product methyl acetate, among others, were calculated based on the conservation of carbon atom moles, with the following results:

$$Con_{DME} = 1 - \frac{2C_{DME}}{2C_{DME} + 2C_{MAc} + C_{MeOH} + \Sigma_i iC_i}$$

$$Sel_{MAc} = \frac{2C_{MAc}}{2C + C_{MeOH} + \Sigma_i iC_i}$$

C_{DME}, C_{MAc} and C_{MeOH} represent the molar concentration of DME, methyl acetate and methanol in the reactor outlet gas, respectively, and C_i represents the molar concentration of hydrocarbons in the reactor outlet gas, and i refers to the number of carbon atoms contained in the hydrocarbon.

Declaration of competing interest

The authors declare no competing interests.

Acknowledgements

The authors are grateful to the financial support provided by the National Key Research and Development Program of China (No. 2022YFE0116000), the National Natural Science Foundation of China (22241801, 22022202, 22032005, 22288101, 21972142, 21991090, 21991092, 21991093), and Dalian Outstanding Young Scientist Foundation (2021RJ01).

Appendix A. Supplementary data

Supplementary data to this article can be found online at https://doi.org/10.1016/j.cjsc.2024.100247.

References

[1] R. Xu, W. Pang, Q. Huo, Molecular Sieves and Porous Material Chemistry, second ed., Science Press, 2004.
[2] W. Loewenstein, The distribution of aluminum in the tetrahedra of silicates and aluminates, Am. Mineral. 39 (1954) 92–96.
[3] R. Xu, Zeolite Molecular Sieves Structure and Synthesis, 1987.
[4] Z. Yuan, W. Zhou, H. Li, Progress in synthesis of zeolite and zeolite-like molecular sieves, Prog. Chem. 13 (2001) 113–117, https://doi.org/10.3321/j.issn:1005-281X.2001.02.006.
[5] W. Wang, C. Zeng, N. Tsubaki, Recent advancements and perspectives of the CO_2 hydrogenation reaction, Green Carbon 1 (2023) 133–145, https://doi.org/10.1016/j.greenca.2023.10.003.
[6] G. Fu, Q. Lang, X. Liu, H. Zhao, Y. Sun, L. Zhao, A. Omran, P. Lu, X. Yang, B. Yu, V. Valtchev, Zeolitic germanosilicate analogue to pharmacosiderite crystallized in an acidic medium, Green Carbon 1 (2023) 185–192, https://doi.org/10.1016/j.greenca.2023.11.003.
[7] S. Zhao, S. He, K. Kim, L. Wang, R. Ryoo, Z. Wang, J. Huang, Influence of hierarchical ZSM-5 catalysts with various acidity on the dehydration of glycerol to acrolein, Magnetic Resonance Letters 1 (2021) 71–80, https://doi.org/10.1016/j.mrl.2021.100002.
[8] X. Li, W. Shen, H. Sun, Solid-state NMR studies of sulfonated SBA-15 and the synergistic catalysis of fructose into 5-hydroxymethylfurfural with dimethyl sulfoxide, Magnetic Resonance Letters 2 (2022) 38–47, https://doi.org/10.1016/j.mrl.2021.11.001.
[9] X. Wang, R. Li, C. Yu, Y. Liu, C. Lu, Influence of acid site distribution on dimethyl ether carbonylation over mordenite, Ind. Eng. Chem. Res. 58 (2019) 18065–18072, https://doi.org/10.1021/acs.iecr.9b02610.
[10] K. Cao, D. Fan, M. Gao, B. Fan, N. Chen, L. Wang, P. Tian, Z. Liu, Recognizing the important role of surface barriers in MOR zeolite catalyzed DME carbonylation reaction, ACS Catal. 12 (2022) 1–7, https://doi.org/10.1021/acscatal.1c04966.
[11] R. Liu, B. Fan, Y. Zhi, C. Liu, S. Xu, Z. Yu, Z. Liu, Dynamic evolution of aluminum coordination environments in mordenite zeolite and their role in the dimethyl ether (DME) carbonylation reaction, Angew. Chem. Int. Ed. 61 (2022) e202210658, https://doi.org/10.1002/anie.202210658.
[12] K. Cao, D. Fan, S. Zeng, B. Fan, Z. Liu, Organic-free synthesis of MOR nano assemblies with excellent DME carbonylation performance, Chin. J. Catal. 42 (2021) 1468–1477, https://doi.org/10.1016/S1872-2067(20)63777-9.
[13] A. Bhan, A.D. Allian, G.J. Sunley, D.J. Law, E. Lglesia, Specificity of sites within eight-membered ring zeolite channels for carbonylation of methyls to acetyls, J. Am. Chem. Soc. 129 (2007) 4919–4924, https://doi.org/10.1021/ja070094d.
[14] Y. Li, S. Huang, Z. Cheng, K. Cai, L. Li, E. Milan, J. Lv, Y. Wang, Q. Sun, X. Ma, Promoting the activity of Ce-incorporated MOR in dimethyl ether carbonylation through tailoring the distribution of Bronsted acids, Appl. Catal. B Environ. 256 (2019) 117777, https://doi.org/10.1016/j.apcatb.2019.117777.
[15] P.K. Bajpai, M.S. Rao, K.V.G.K. Gokhale, Synthesis of mordenite type zeolite using silica from rice husk ash, Ind. Eng. Chem. Prod. Res. Dev. 20 (1981) 721–726, https://doi.org/10.1021/i300004a026.
[16] E. Zhan, Z. Xiong, W. Shen, Dimethyl ether carbonylation over zeolites, J. Energy Chem. 36 (2019) 51–63, https://doi.org/10.1016/j.jechem.2019.04.015.
[17] M. Boronat, C. Martinez-Sanchez, D. Law, A. Corma, Enzyme-like specificity in zeolites: a unique site position in mordenite for selective carbonylation of methanol and dimethyl ether with CO, J. Am. Chem. Soc. 130 (2008) 16316–16323, https://doi.org/10.1021/ja805607m.
[18] P. Cheung, A. Bhan, G.J. Sunley, E. Iglesia, Selective carbonylation of dimethyl ether to methyl acetate catalyzed by acidic zeolites, Angew. Chem. Int. Ed. 45 (2006) 1617–1620, https://doi.org/10.1002/anie.200503898.
[19] P. Cheung, A. Bhan, G.J. Sunley, D.J. Law, E. Iglesia, Site requirements and elementary steps in dimethyl ether carbonylation catalyzed by acidic zeolites, J. Catal. 245 (2015) 110–123, https://doi.org/10.1016/j.jcat.2006.09.020.
[20] J. Yijiao, H. Michael, W. Wei, On the reactivity of surface methoxy species in acidic zeolites, J. Am. Chem. Soc. 128 (2006) 11679–11692, https://doi.org/10.1021/JA061018Y.
[21] Y. Chu, A.Y. Lo, C. Wang, F. Deng, Origin of high selectivity of dimethyl ether carbonylation in the eight-membered ring channel of mordenite zeolite, J. Phys. Chem. C 123 (2019) 15503–15512, https://doi.org/10.1021/acs.jpcc.9b01874.
[22] T. Blasco, M. Boronat, P. Concepción, A. Corma, D. Law, J.A. Vidal-Moya, Carbonylation of methanol on metal-acid zeolites: evidence for a mechanism involving a multisite active center, Angew. Chem. Int. Ed. 46 (2007) 3938–3941, https://doi.org/10.1002/anie.200700029.
[23] T. He, P. Ren, X. Liu, S. Xu, X. Han, X. Bao, Direct observation of DME carbonylation in the different channels of H-MOR zeolite by continuous-flow solid-state NMR spectroscopy, Chem. Commun. 51 (2015) 16868–16870, https://doi.org/10.1039/c5cc07201h.
[24] B. Li, J. Xu, B. Han, X. Wang, G. Qi, Z. Zhang, C. Wang, F. Deng, Insight into dimethyl ether carbonylation reaction over mordenite zeolite from *in-situ* solid-state NMR spectroscopy, J. Phys. Chem. C 117 (2013) 5840–5847, https://doi.org/10.1021/jp400331m.
[25] H.R. Gerberich, W.K. Hall, Studies of the hydrogen held by solids: IX. The hydroxyl groups of alumina and silica-alumina as sites for the isomerization of butene, J. Catal. 5 (1966) 99–110, https://doi.org/10.1016/S0021-9517(66)80129-X.
[26] P.Y. Dapsens, C. Mondelli, J. Pérez-Ramírez, Design of Lewis-acid centres in zeolitic matrices for the conversion of renewables, Chem. Soc. Rev. 44 (2015) 7025–7043, https://doi.org/10.1039/C5CS00028A.
[27] R. Otomo, T. Yokoi, J.N. Kondo, T. Tatsumi, Dealuminated beta zeolite as effective bifunctional catalyst for direct transformation of glucose to 5-hydroxymethylfurfural, Appl. Catal. Gen. 470 (2014) 318–326, https://doi.org/10.1016/j.apcata.2013.11.012.
[28] S. Suganuma, T. Hisazumi, K. Taruya, E. Tsuji, N. Katada, Influence of acidic property on catalytic activity and selectivity in dehydration of glycerol, ChemistrySelect 2 (2017) 5524–5531, https://doi.org/10.1002/slct.201700941.
[29] K. Chen, S. Horstmeier, V.T. Nguyen, B. Wang, S.P. Crossley, T. Pham, Z. Gan, I. Hung, J.L. White, Structure and catalytic characterization of a second framework Al(IV) site in zeolite catalysts revealed by NMR at 35.2 T, J. Am. Chem. Soc. 142 (2020) 7514–7523, https://doi.org/10.1021/jacs.0c00590.
[30] L. He, J. Li, S. Han, D. Fan, X. Li, S. Xu, Y. Wei, Z. Liu, Dynamic evolution of HZSM-5 zeolite framework under steam treatment, Chemical Synthesis 3 (2023) 54, https://doi.org/10.20517/cs.2023.55.
[31] M. Ravi, V.L. Sushkevich, J.A. van Bokhoven, Towards a better understanding of Lewis acidic aluminium in zeolites, Nat. Mater. 19 (2020) 1047–1056, https://doi.org/10.1038/s41563-020-0751-3.
[32] H. Xue, X. Huang, E. Ditzel, E. Zhan, M. Ma, W. Shen, Dimethyl ether carbonylation to methyl acetate over nanosized mordenites, Ind. Eng. Chem. Res. 52 (2013) 11510–11515, https://doi.org/10.1021/ie400909u.
[33] S. Wang, W. Guo, L. Zhu, H. Wang, K. Qiu, K. Cen, Methyl acetate synthesis from dimethyl ether carbonylation over mordenite modified by cation exchange, J. Phys. Chem. C 119 (2014) 524–533, https://doi.org/10.1021/jp511543x.
[34] S. Liu, H. Liu, X. Ma, Y. Liu, W. Zhu, Z. Liu, Identifying and controlling the acid site distributions in mordenite zeolite for dimethyl ether carbonylation reaction by means of selective ion-exchange, Catal. Sci. Technol. 10 (2020) 4663–4672, https://doi.org/10.1039/d0cy00125b.
[35] K. Cao, D. Fan, L. Li, B. Fan, L. Wang, D. Zhu, Q. Wang, P. Tian, Z. Liu, Insights into the pyridine-modified MOR zeolite catalysts for DME carbonylation, ACS Catal. 10 (2020) 3372–3380, https://doi.org/10.1021/acscatal.9b04890.
[36] A. Yakimov, M. Ravi, R. Verel, V.L. Sushkevich, J.A. van Bokhoven, C. Copéret, Structure and framework association of Lewis acid sites in MOR zeolite, J. Am. Chem. Soc. 144 (2022) 10377–10385, https://doi.org/10.1021/jacs.2c02212.
[37] X. Wang, R. Li, C. Yu, Y. Liu, L. Zhang, C. Xu, H. Zhou, Enhancing the dimethyl ether carbonylation performance over mordenite catalysts by simple alkaline treatment, Fuel 239 (2019) 794–803, https://doi.org/10.1016/j.fuel.2018.10.147.
[38] A. Reule, J. Sawada, N. Semagina, Effect of selective 4-membered ring dealumination on mordenite-catalyzed dimethyl ether carbonylation, J. Catal. 349 (2017) 98–109, https://doi.org/10.1016/j.jcat.2017.03.010.
[39] M. Müller, G. Harvey, R. Prins, Comparison of the dealumination of zeolites beta, mordenite, ZSM-5 and ferrierite by thermal treatment, leaching with oxalic

acid and treatment with $SiCl_4$ by ^{1}H, ^{29}Si and ^{27}Al MAS NMR, Microporous Mesoporous Mater. 34 (2000) 135–147, https://doi.org/10.1016/S1387-1811(99)00167-5.
[40] D. Sandström, M.H. Levitt, Structure and molecular ordering of a nematic liquid crystal studied by natural-abundance double-quantum ^{13}C NMR, J. Am. Chem. Soc. 118 (1996) 6966–6974, https://doi.org/10.1021/ja9601853.
[41] T. Gullion, J. Schaefer, Rotational-echo double-resonance NMR, J. Magn. Reson. 81 (1989) 196–200, https://doi.org/10.1016/0022-2364(89)90280-1.
[42] X. Yao, Z. Zhao, G. Hou, Development of *in situ* MAS NMR and its applications in material synthesis and heterogeneous catalysis, Chin. J. Struct. Chem. 41 (2022) 2210045–2210055, https://doi.org/10.14102/j.cnki.0254-5861.2022-0166.
[43] L. Guo, R. Song, Rare-earth metal dialkyl complexes supported by 1,3-disubstituted indolyl ligand: synthesis, characterization and catalytic activity for isoprene polymerization, Chin. J. Struct. Chem. 40 (2021) 1055–1060, https://doi.org/10.14102/j.cnki.0254-5861.2011-3172.
[44] X. Bai, J. Zhang, C. Liu, S. Xu, Y. Wei, Z. Liu, Solid-state NMR study on dealumination mechanism of H-MOR zeolite by high-temperature hydrothermal treatment, Microporous Mesoporous Mater 354 (2023) 112555, https://doi.org/10.1016/j.micromeso.2023.112555.
[45] T.H. Chen, B.H. Wouters, P.J. Grobet, Aluminium coordinations in zeolite mordenite by 27Al multiple quantum MAS NMR spectroscopy, Eur. J. Inorg. Chem. 21 (2000) 281–285, https://doi.org/10.1002/(SICI)1099-0682(200002)2000:2<281::AID-EJIC281>3.0.CO;2-I.
[46] T.H. Chen, K. Houthoofd, P.J. Grobet, Toward the aluminum coordination in dealuminated mordenite and amorphous silica-alumina: a high resolution 27Al MAS and MQ MAS NMR study, Microporous Mesoporous Mater. 86 (2005) 31–37, https://doi.org/10.1016/j.micromeso.2005.07.005.
[47] M. Ravi, V.L. Sushkevich, J.A. van Bokhoven, On the location of Lewis acidic aluminum in zeolite mordenite and the role of framework-associated aluminum in mediating the switch between Bronsted and Lewis acidity, Chem. Sci. 12 (2021) 4094–4103, https://doi.org/10.1039/d0sc06130a.
[48] M. Dyballa, D.K. Pappas, K. Kvande, E. Borfecchia, B. Arstad, P. Beato, U. Olsbye, S. Svelle, On how copper mordenite properties govern the framework stability and activity in the methane-to-methanol conversion, ACS Catal. 9 (2019) 365–375, https://doi.org/10.1021/acscatal.8b04437.
[49] C.A. Fyfe, G.C. Gobbi, W.J. Murphy, Investigation of the contributions to the silicon-29 MAS NMR line widths of zeolites and detection of crystallographically inequivalent sites by the study of highly siliceous zeolites, J. Am. Chem. Soc. 106 (1984) 4435–4438, https://doi.org/10.1021/ja00328a024.
[50] D. Kennes, H.N. Abubackar, M. Diaz, M.C. Veiga, C. Kennes, Bioethanol production from biomass: carbohydrate vs syngas fermentation, J. Chem. Technol. Biotechnol. 91 (2015) 304–317, https://doi.org/10.1002/jctb.4842.
[51] R. Liu, S. Zeng, T. Sun, S. Xu, Z. Yu, Y. Wei, Z. Liu, Selective removal of acid sites in mordenite zeolite by trimethylchlorosilane silylation to improve dimethyl ether carbonylation stability, ACS Catal. 12 (2022) 4491–4500, https://doi.org/10.1021/acscatal.1c05896.
[52] J. Zhang, X. Ding, H. Liu, D. Fan, S. Xu, Y. Wei, Z. Liu, Study on the framework aluminum distributions of HMOR zeolite and identification of active sites for dimethyl ether carbonylation reaction, Acta Chim. Sinica 80 (2022) 590–597, https://doi.org/10.6023/a22010014.
[53] C. Liu, S. Xu, Y. Wei, Z. Liu, Effect of high temperature steam heat treatment on the framework aluminum stability of H-MOR zeolite, Acta Pet. Sin. 39 (2023) 1231–1241, https://doi.org/10.3969/j.issn.1001-8719.2023.06.002.